Shahrood University of Technology

Journal of Mining and Environment (JME)

Journal homepage: www.jme.shahroodut.ac.ir

Iranian Society of Mining Engineering (IRSME)

# A Promising Automatic System for studying of Coal Mine Surfaces using Sentinel-2 Data to Assess a Classification on a Pixel-based Pattern

Ajay Kumar

*Department of Computer Science and Engineering, School of Computer Science and Engineering, Manipal University Jaipur, Rajasthan, India*

***Article Info***

*Received 9 May 2023*

*Received in Revised form 27 June 2023*

*Accepted 19 September 2023*

*Published online 19 September 2023*

*DOI: 10.22044/jme.2023.13064.2380*

***Keywords***

*Remote Sensing Image*

*Artificial Neural Networks*

*Dataset*

*Land Use*

*Machine learning*

***Abstract***

Land use (LU) classification based on remote sensing images is a challenging task that can be effectively addressed using a learning framework. However, accurately classifying pixels according to their land use poses a significant difficulty. Despite advancements in feature extraction techniques, the effectiveness of learning algorithms can vary considerably. In this study conducted in Talcher, Odisha, India, the researchers proposed the use of Artificial Neural Networks (ANNs) to classify land use based on a dataset collected by the Sentinel-2 satellite. The study focused on the Talcher region, which was divided into five distinct land use classes: coal area, built-up area, barren area, vegetation area, and waterbody area. By applying ANNs to the mining region of Talcher, the researchers aimed to improve the accuracy of land use classification. The results obtained from the study demonstrated an overall accuracy of 79.4%. This research work highlights the importance of utilizing remote sensing images and a learning framework to address the challenges associated with pixel-based land use classification. By employing ANNs and leveraging the dataset from the Sentinel-2 satellite, the study offers valuable insights into effectively classifying different land use categories in the Talcher region of India. The findings contribute to the advancement of techniques for accurate land use analysis, with potential applications in various fields such as urban planning, environmental monitoring, and resource management.

## 1. Introduction

The mining of land does have a wide variety of effects on people, animals, and the natural resources that are available. In addition to natural risks, fauna, flora, and natural resources, much of the land has been mined for fossil fuels including coal, oil, and metal. This has led to the extinction of many species [1]. In addition, the information on mining land takes into consideration socio-demographic data, which is often regarded as an essential component of planning and management [2]. Besides, it offers significant information about mining regions, which is essential for comprehending the intricate connections between coal mining regions and other places [2]. A high proportion of open-source satellite images are widely used as a result of cutting-edge remote sensing technology, presenting new possibilities for mining LU information [3]. However, the spatial features of mining terrain observed using satellite imagery are extremely complex and multi-faceted, conflating various other surfaces (built-up areas, barren areas, etc.). Due to the diversity and complexity of spatial features, classifying mined regions into different LU classes is an extremely challenging task. Therefore, by precisely defining the spatial patterns or structures in the satellite perception data, a reliable and robust mining LU classification technique must be devised.

LU classifications are significantly affected due to the demand and supply of human needs over land use and their fulfilment of desires. Conventional methods are challenging work for the estimation of LU patterns classification by field survey over large area coverage, and thus the remote sensing

Corresponding author: ajay3789@gmail.com (A. Kumar)

approaches with computer vision are the most appropriate. These remote sensing images are used for classification viz. pixel-based and object-based [4]. Also the pixel-based is suitable for low spatial resolution data, whereas the object-based is suitable for high spatial resolution data [4]. In the last few decades, many research has developed an artificial intelligence algorithm for image processing [6], classification [7], and detection [8]. The developed algorithms generally follow classification viz. supervised [9], unsupervised [10], semi-supervised [11], and reinforcement [12] for learning of images. The developed model of supervised image classification (SIC) is the process of data by mapping input and output, and unsupervised image classification (UIC) is the process of data only the input and no corresponding output [13]. SIC algorithms are McCulloch-Pitts model (MCPs) [14], First Perceptron [15], Back-Propagation [16], Boltzmann Machine [17], Restricted Boltzmann Machine [18], Gradient Descent [19], etc., whereas UIC algorithms are Hebbian learning model [20], K-means clustering model [21], singular value decomposition [22], generative learning models [24], hierarchical clustering model [24], principal component analysis [25], etc. Also the developed model has its own merits and demerits, and no model provides prediction with a hundred percent accuracy. Moreover, all the algorithms require multiple steps of image processing for classifications. Thus it needs the time-to-time implementation of the design and development of automated LU classification of remote sensing imagery with more accuracy. ANNs is solved a realistic spatial features pattern in a remote sensing image. These patterns are categorized in two ways dynamic, nature adaptive [26], and non-adaptive [27]. Thus it is the greatest hit with neural networks by adaptive patterns techniques. This is many applications related to adaptive patterns used in remote sensing imagery like impacts on the environment and disasters [28], slope susceptibility, and deforestation [29]. ANNs have expert learning systems for the capability of spatial patterns to identify unknown patterns by image-based training models [30]. Moreover, it has forecasted certain outcomes by extrapolation, and their importance is considerable for LU pattern classification [31]. ANNs can be used for image classification based on automatic feature extractions [32] from the image in contrast to other traditional classifiers. In conventional classifiers [33], multiple spatial interactions between pixels are loosed, which ANNs can effectively do without losing information. In this study, an ANNs technique was utilised in remote sensing image analysis to classify spatial characteristics patterns of remote sensing imaging including coal mining area, waterbody, built-up areas, barren land, and vegetation area. The application of SIC is used for training and testing images to classify the patterns. The utilization of ANNs is driven by the fact that similar to a human brain, they are able to learn relevant features from several levels of remote-sensing images and can collect relevant features themselves.

A neural net is a network of neurons that also includes synoptic data information. Even satellite image feature patterns are discovered based on ANN mining techniques for LU classification using remote sensing images. When compared to other models, ANNs models are frequently found to provide a higher overall classification accuracy; however, they are not always effective in all situations. The fast gradient descent model improves the model at the quadratic convergence rate o(k2) to address neural network issues in image classification. The findings were 97.54%, 95.59%, 0.31, and 83.17 in terms of training accuracy, test accuracy, lost cost, and CPU times, respectively [34]. Using a hyperspectral image, the Gaussian-Bernoulli restricted Boltzmann machine (GBRBM) was used to classify mining areas. This GBRBMs model employs a logistic regression layer for classification and many hidden layers to extract deep features. Instead of dataset improvements of 5%–10%, GBRBMs in parallel produce overall accuracy increases of roughly 2%–5% [18]. A study comparing the use of neural networks and statistics for picture categorization in land cover mapping. Both image classifications yielded 91.6% for the neural network classification and 88.6% for the statistical (maximum likelihood) classification [35]. With the use of a backpropagation technique, ANNs-based distant sensed picture change detection was trained. 95.6% of changes in land cover could be detected accurately, according to the results [35]. A neural-object-based ANN and random forest model with minimal parameters and hyperparameters. Sana'a's 2016 city map incorporates Sentinel-2A and Landsat-8 multispectral satellite images and a normalized digital elevation model. This model produced 7–10-layer neural networks with 1,000–million simulated neurons [51]. Maximum likelihood classifier and cellular automata-Markov models predict 2030 and 2050 LULC trends. Also in the years 1990, 2000, 2010, and 2020 classified images were 90%, 92%, 93%, and 91% accurate

[52]. Transition potential modeling anticipated cellular automata-ANN LULC alterations. Landsat data of the year 2022, real and simulated LULC data yielded 86.53% accuracy and 0.82 kappa [53]. TerrSet's Cellular Automata-Markov Chain model derived 2035 and 2050 of the LULC. GRB's LULC dynamics might last for years, according to experts. Forests, shrubs, and grasslands vanished while agriculture, habitation, and water increased. Unsustainable land use degraded it [54]. Landsat images spectral signature and feature extraction of land-use classifications. This imaging file includes three images from Landsat satellite sensors from 2003 to 2017. It assesses crop, vegetation, and orchard health using the vegetation index (VI). For 2017, 2010, and 2003, ANNs classification accuracy was 90.10%, 75.75%, and 78.37% [55]. This article serves as a survey of recent ANNs LU classification methods. It is driven to become familiar with the ANNs model used in the mining industry and to offer innovative ideas for the sector's growth.

## 2. Materials and Methods

### 2.1. Studied area

The study site demonstrated a sub-area of the mining region Talcher Coalfield located in the Angul District of Odisha State. The study location is geographically represented as shown in Figure 1, at the centre of Angul District lies latitude $20.95^0$N and longitude $85.23^0$E. The Geological Survey of India estimates 38.65 billion tonnes of coal reserves in the Talcher Coalfield, India's most notable coal resource. Additionally, the coalfield is separated into five distinct producing areas Talcher, Jagannath, Kalinga, Lingaraj, and Hingula across its 500 $km^2$ cover [36].

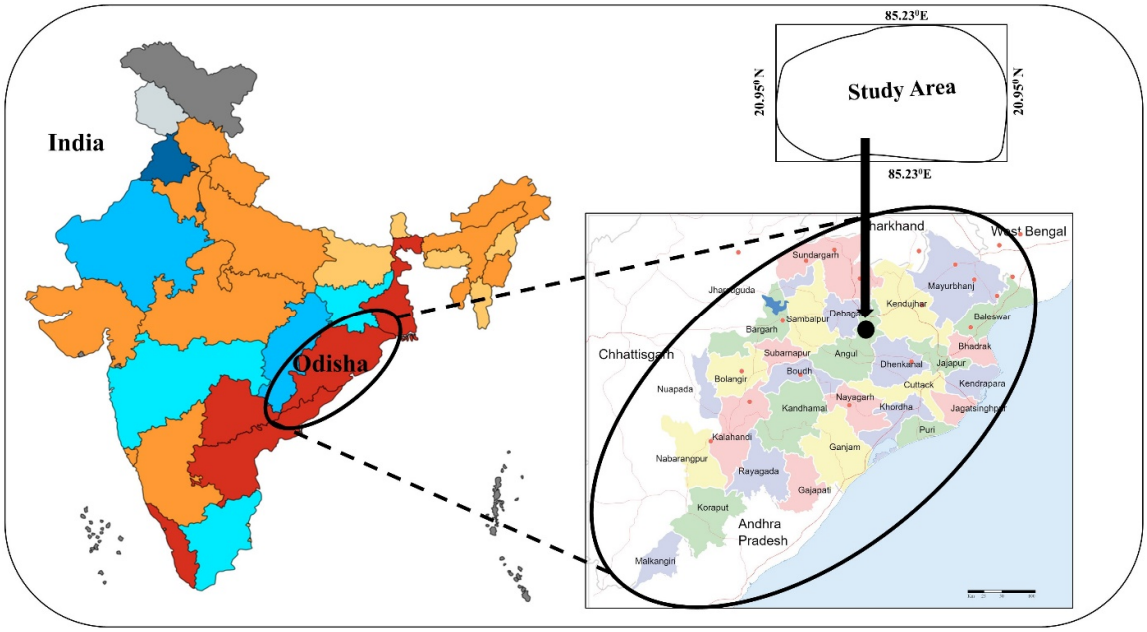


**Figure 1. Studied area of sub-part of Talcher coalfield, Odisha.**

### 2.2. Labelling and generation of image dataset

Acquiring satellite data from different sources is the preliminary and pivotal stage in the LU classification (https://earthexplorer.usgs.gov). In the present study, the LU analysis will make use of data from the Sentinel-2A satellite that was acquired in the year 2019. Sentinel-2A is a component of the Copernicus Programme that was developed by the European Union (EU), and is responsible for the systematic acquisition of optical imagery with a high spatial resolution (10 m to 60 m) over land and coastal seas. Data across the three visible bands (red, green, and blue) is layered to generate a single band that can be used to categorize features. Table 1 contains an in-depth breakdown of the data's properties and qualities (https://gisgeography.com/sentinel-2-bands-combinations/). Image pre-processing involves processing raw satellite data. It does this by either lowering the amount of distortion in the satellite picture or increasing the number of features that can be processed and analysed [38]. The satellite data that was collected from the relevant government agency is in the form of an array of pixel values, and each pixel possesses the property

of a scene that was measured over a specific geographic region [39]. The study primarily examined the average brightness of the imagery after it was filtered through red, green, and blue bands [40]. Although there is a large quantity of image data already available, this was the focus of the research. The values of the pixels occupying the image are all preserved as an 8-bit integer, and their range of possible values is ranging from 0 to 256, depending on the brightness [41]. In the pre-processing of images, cropping the image [42] and filtering the image [43] are both included, and it is possible to evaluate the area of interest (AOI) by excluding irrelevant segments of the image that are displayed.

**Table 1. Characteristics of Sentinel-2 data in visible bands.**

| Sl. No | Bands | Central wavelength (nm) | Resolution (m) |
|---|---|---|---|
| 1 | Band 2 (Blue) | 492.4 | 10 |
| 2 | Band 3 (Green) | 559.8 | 10 |
| 3 | Band 4 (Red) | 664.6 | 10 |

The process of creating the dataset involves extracting smaller, class-specific images from larger-scale imagery, resulting in a comprehensive collection of sub-scale images for various classes. By analysing the pixel values of surface spatial features, sub-scale imagery was produced, revealing a remarkable variation in distinct classes. This ensuing collection of images is truly comprehensive, covering a diverse range of classes. Also the database was generated by cropping the 3-band composite image into a scale of (10∗10) sub-image for five different classes viz. coal area, barren area, built-up area, water area, and vegetation area. A total of 100 cropped images derived for each class have represented a sample of cropped images as shown in Figure 2. Entirely these images are labelled in a regular scale size of array form such as [10,10,3], where 10 pixels of width,10 pixels of height and 3 channel.

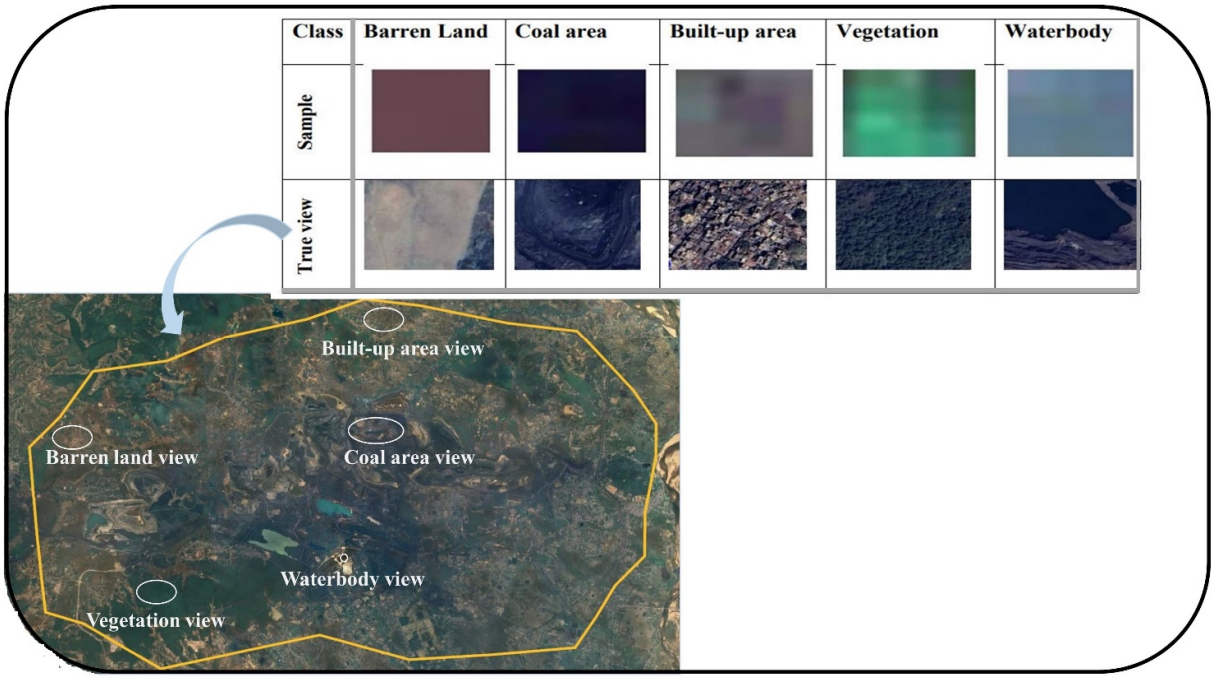


**Figure 2. Benchmark of remote sensing image of scale size [10, 10, 3] for sample class of spatial features and true view of google earth image.**

### 2.3. Methodology

The process of promising an automatic system for the studying of coal mine surfaces using a satellite data flowchart is shown in Figure 3.

#### 2.3.1. ANNs architecture

For the study of LU classification in remote sensing images, this research endeavour to design an ANNs algorithm is being applied [50]. In the same approach that the human visual brain processes information, the training dataset is processed into an ANNs model for LU classification [43]. ANNs are strong computational frameworks that explore the essential dynamics that drive neural networks and reveal the approaches used at each level, revealing their transformational potential. These complicated webs of linked nodes have shown exceptional skills in modelling complex patterns and deriving significant insights from data. This sample dataset possesses a collection of precisely 500 sample patches, which have been sensibly allocated among the realms of training, validation, and testing, adhering to a harmonious distribution ratio of 70% for training and an equally significant 30% for validation or testing purposes. In addition to that, this consists of three parameters of layers, all of which are tied to the weights of the layers and are shared throughout the input indicated in Table 2. Figure 4 depicts a class of feedforward network structure called the three-layer perceptron, that can be found [44]. In the end, it is depicted as one feed-forward network among five outputs on the output layer via processing an activation function. It also includes a hidden layer.

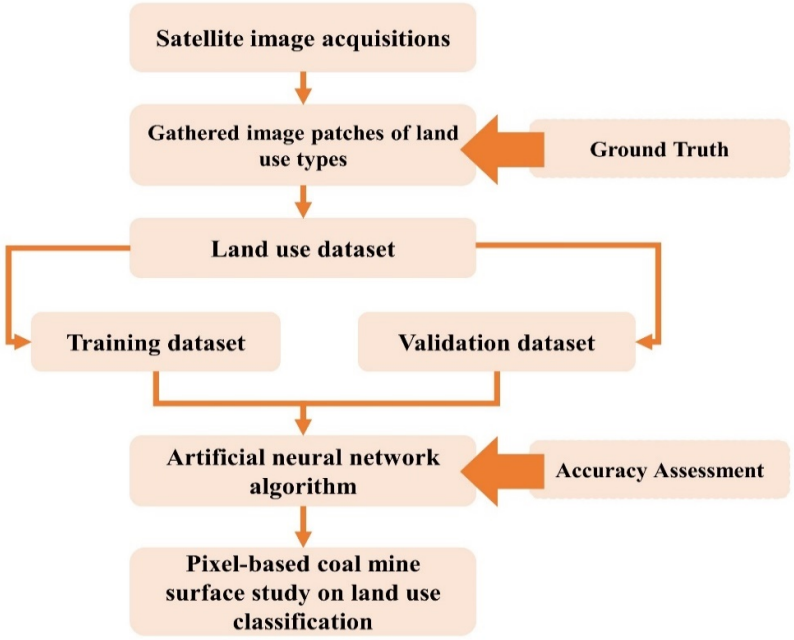


**Figure 3. Adopted flowchart of pixel-based pattern coal mine surface study on land use classification.**

**Table 2. Parameter setting of ANNs layers.**

| Sl. No | Layer name | Description | Neurons |
|---|---|---|---|
| 1 | Input | 10*10*3 scale size of images, number of 500 images sample collected into dataset. Each class has 100 image sample among five class viz. Coal mining area, Built-up area, Barren area, vegetation area and water body | 300 |
| 2 | Hidden | Colum/row wise arrangement of spatial feature value and synapse of information by neural network passes. | 40 |
| 3 | Output | Classified five class viz. viz. Coal mining area, Built-up area, Barren area, vegetation area and water body | 5 |

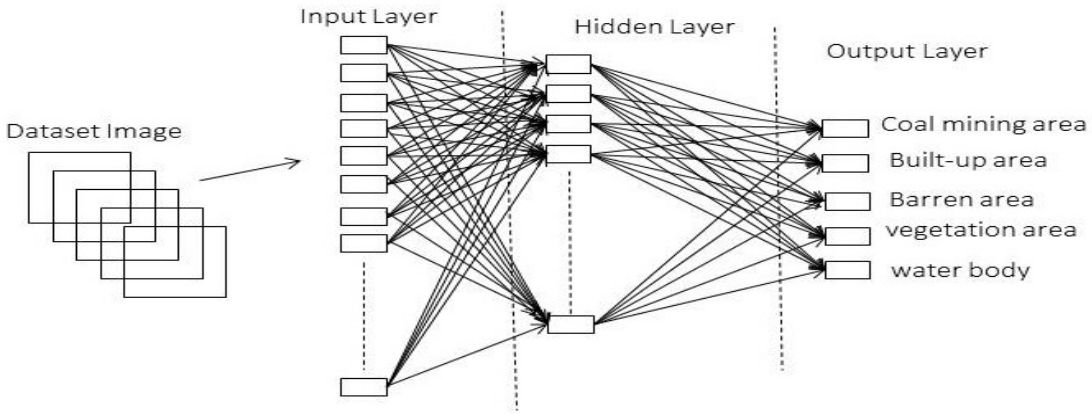


**Figure 4. ANNs learning framework of mining activities region.**

Training outlines ANNs capabilities, gradient descent, and a well-chosen training dataset alter the network's weights and biases repeatedly. The network refines its parameters via backpropagation and forward propagation to reduce the difference between expected and actual outputs. The training step helps the ANN learn complex patterns from the training data. The efficiency and scalability of ANNs must be tested. Likewise, the network is put through its paces utilizing data that wasn't part of its training. The model's resilience and adaptability to new data may be measured by accuracy, precision, recall, and the F1 score. It could potentially be worthwhile to verify the network's capabilities outside of the training set using cross-validation methods like as k-fold validation in an attempt to boost the reliability of the evaluation. Cross-validation is an example of a practice that may be used.

The feed-forward ANNs [45], the input dataset $x_i$ of images are followed for input network and directly connected to the output layer nodes $l_1$, $l_2$, $l_3$, $l_4$, $l_5$ . These output nodes are used activation function $A_1$, $A_2$, $A_3$, $A_4$, $A_5$ to yield the output $o_1$, $o_2, o_3, o_4, o_5$ represented in Equations (1) to (5).

$$o_1 = A_1(l_1) = A_1\left(\sum_{i=1}^{300} w_{1,i}x_i + b_1\right) \quad (1)$$

$$o_2 = A_2(l_2) = A_2\left(\sum_{i=1}^{300} w_{2,i}x_i + b_2\right) \quad (2)$$

$$o_3 = A_3(l_3) = A_3\left(\sum_{i=1}^{300} w_{3,i}x_i + b_3\right) \quad (3)$$

$$o_4 = A_4(l_4) = A_4\left(\sum_{i=1}^{300} w_{4,i}x_i + b_4\right) \quad (4)$$

$$o_5 = A_5(l_5) = A_5\left(\sum_{i=1}^{300} w_{5,i}x_i + b_5\right) \quad (5)$$

The activation function $A_{i=1,2,3,4,5}$ are varies from the feed forward neural network of weight $w_{i=1,2,3,4,5}$ with depends upon condition of bias $b_{1=1,2,3,4,5}$ to fit for network. Generally, feed forward network is applied activation function based on linear and logistic (sigmoid) due to instead of structure three layers [45]. Also the stochastic gradient descent (SGD) is most popular computing model of gradients represented a graphically of loss/cost function based on performance of neural network [34]. Here, neurons are represented in input layer act as buffer for transferring the input data to neurons in hidden layer. After that, each active neuron $j$ in the hidden layer sums up its input dataset $x_1$ after feed a weighting them with the strengths of the particular connections $w_{j,i}$ from the input layer. The end is done output $o_i$ calculated by function $f$ of the sum as similar Equation (6).

$$o_i = f\left(\sum_{i=1}^{n} w_{j,i}x_i\right) \quad (6)$$

Similar, the backpropagation SGD [48] is provides to alter $\Delta w_{j,i}$ the weight of connection between neurons $i$ and $j$ as Equation (7). The representation of $\gamma, \delta_j$ is learning rate, a factor depending on neurons $j$ as input or hidden neurons.

$$\Delta w_{j,i} = \gamma \delta_j x_i \quad (7)$$

Also more prospective representation of $\delta_j$ is encountered the terms in Equation (8). $\partial nnet_j$ as the aggregate weighted summarization of input dataset to neurons $j$ with time $t$ , $o_j^{(t)}$ as the target output for neurons $j$.

$$\delta_j = \left(\frac{\partial f}{\partial nnet_j}\right)( o_j^{(t)} - o_j) \quad (8)$$

Computing error is impotence of SGD model but it is useful in layered feed forward neural network training so that a greater number of iterations are required for changing the weights. Sometimes, weight decay is happened due to penalize the weights of hidden neurons. This weight decay is resolved and prevents the neural network fitting. This is used a simplest error function ($\xi$) in Equations (9) to (12), where an initial error function $\xi_i$ is sum of squared difference between actual and predicated outcome values, $c$ is a positive constant and remaining parameter as explained previously.

$$\xi = \xi_i + c\sum_i\sum_j w_{i,j}^2 \quad (9)$$

Let us assume for the SGD to minimize error, so there are required the changed weight update rule [49] and put $n^{th}$ iteration in equation (10). After that, the mathematical induction is applied in equation (11) and further, expressed to hold iteration for true in equation (12).

$$\Delta w_{i,j}(n^{th}\ iteration) = -\gamma(\frac{\partial \xi}{\partial w_{i,j}})(n^{th} iteration) \quad (10)$$

$$\Delta w_{i,j}(n^{th}\ iteration) = -\gamma\left(\frac{\partial \xi}{\partial w_{i,j}}\right)(n^{th} iteration) - 2c\gamma w_{i,j}(n^{th} iteration) \quad (11)$$

$$\Delta w_{i,j}(n^{th}\ iteration) = -\gamma\left(\frac{\partial \xi}{\partial w_{i,j}}\right)(n^{th} iteration) - (1 - 2c\gamma w_{i,j})(n^{th} iteration) \quad (12)$$

Now, $|1 - 2c\gamma w_{i,j}| < 1$, the condition is represented weighted decreases tend to zero. Thus it is allowed for large weights to carry on while small weight. Similarly, vice versa of error function is used as reciprocal of weights then allow small weights to carry on while large weights tend to zero.

### 2.3.2 Accuracy assessment of an automated classification system

An assessment of the model's ability to predict was carried out with reference to the following indices: accuracy, precision, recall, and F1-score [56]. All of the indices were computed by leveraging the use of the confusion matrix's properties, as shown in the Equations (13)-(16).

$$\text{Accuracy} = \frac{(\text{TP} + \text{TN})}{(\text{TP} + \text{FP} + \text{TN} + \text{FN})} \quad (13)$$

$$\text{Precision} = \frac{(\text{TP})}{(\text{TP} + \text{FP})} \quad (14)$$

$$\text{Recall} = \frac{(\text{TP})}{(\text{TP} + \text{FN})} \quad (15)$$

$$\text{F1-Score} = \frac{(2 \times \text{Precision} \times \text{Recall})}{(\text{Precision} + \text{Recall})} \quad (16)$$

Where, prediction measures terms include TP (true positives), TN (true negatives), FP (false positives), and FN (false negatives).

## 3. Results and Discussion

Our proposed ANNs model is a meticulously compiled and powerful tool that accurately maps datasets for LU classification. There was a carefully split labelled dataset into a training set (consisting of 70% of the data) and a testing set (consisting of 30% of the data) to improve our model's accuracy and dependability. At the beginning of the training process, the network weights are initialized to small, random values. The weight modification process is carefully designed to ensure that the network produces a coherent and dependable output across a diverse range of dataset categories. Thus it is closely analysed the model's performance on the training dataset and observed a steady increase in classification accuracy with each iteration, up to a certain point, after which the accuracy levelled off and remained constant.

Figure 5 (a) depicted the performance plot for our time evaluation model, featuring three distinct curves that illustrate the evolution of mean squared error (MSE) across training, testing, and validation

epochs. After an exhaustive analysis of the model's performance, they were pleased to discover that it achieved its best validation results with an impressively low MSE of 0.10765, which occurred at the 33rd epoch and is denoted by a prominent vertical dash line.

As expected, the network demonstrated superior performance during the training stage as compared to the testing stage since the test data's desired outputs are inherently unknown to the network. Therefore, it utilizes the gradient descent technique to find the spatial feature with the lowest level of error to ensure reliable LU classification. Epoch is defined as the iteration required to perform learning, which is determined by the learning rate or gradient shown in Figure 5(b). Here, the gradient increases and then decreases the number of epochs, but it reaches 0.13196 at 39 epochs. Additionally, validation checks are dependent upon validation failure 6 within the learning rate at 39 epochs.

Besides, it is also examined the error histogram of the trained neural network for the training, validation, and testing steps. As shown in Figure 5(c), the data fitting errors are distributed within a reasonably good range around zero. These are represented that most of bar graph the measurements fall within value of error -0.02665, with a peak at 400 instances. Moreover, the error histogram indicates that the measurements are relatively accurate and consistent, with only a few measurements having significant errors. Also, it is identified patterns and trends in the data and takes corrective action to improve the accuracy of the measurements.

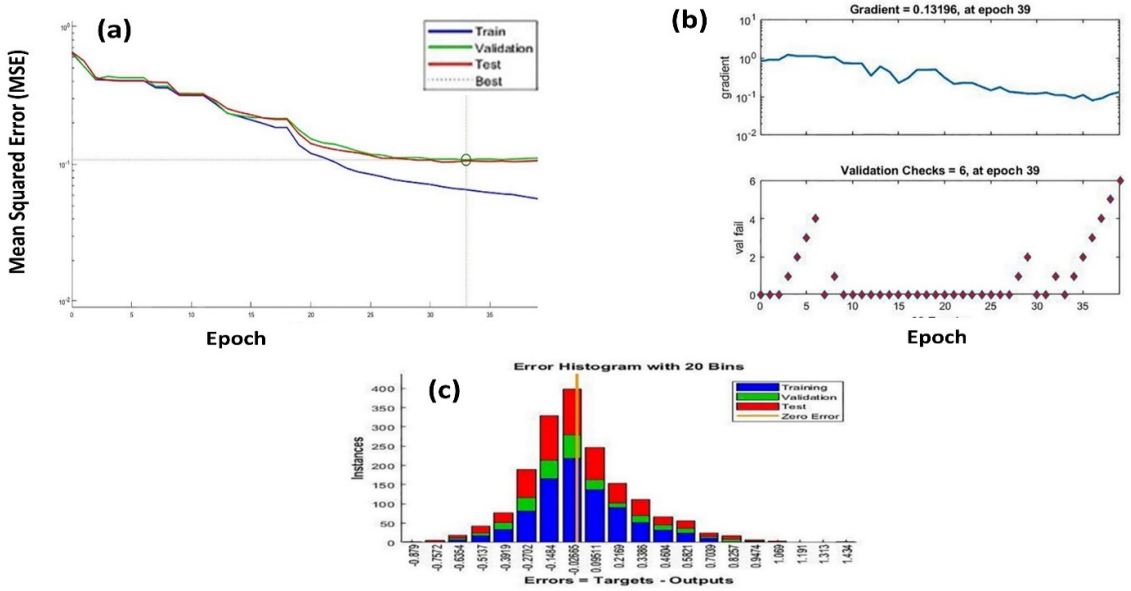


**Figure 5. Tracking the dynamic performance: (a) MSE across epochs for training, testing, validation, (b) Gradient and validation checks (validation failure), and (c) the distribution of errors using the error histogram.**

The efficacy of the ANNs model is evaluated with the aid of the confusion matrix, which is able to be seen in Figure 6. This confusion matrix also includes different categories of barren areas, coal mining area, built-up area, vegetation area and water body. As a way to achieve this accurate examination of the model, it is split up into training, and validation matrix. Its contrast performance in confusion matrices, namely training, and validation accuracy was 88%, and 73.6%, respectively.

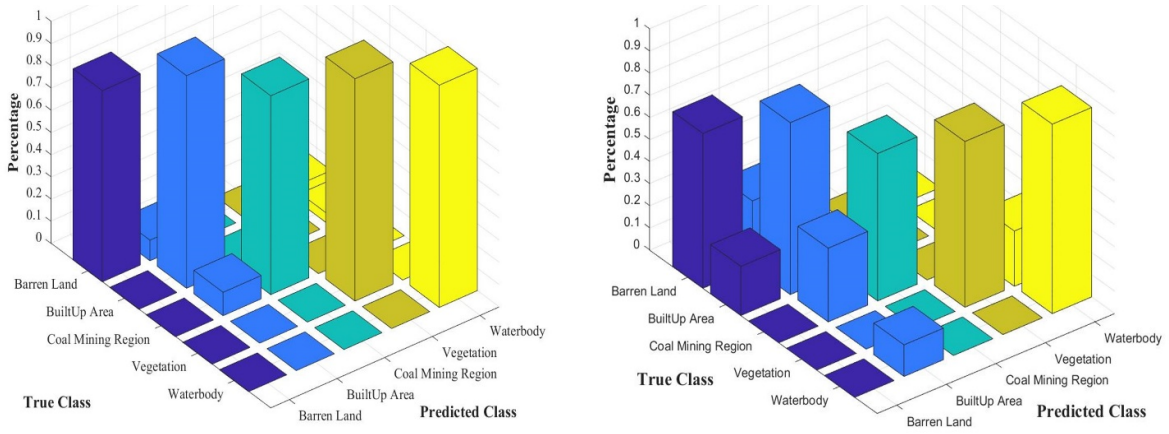


a) Training Confusion Matrix b) Validation Confusion Matrix

**Figure 6. Estimation of the classifier accuracy: (a) Training confusion matrix, and (b) Validation confusion matrix.**

Table 3 presents insightful metrics on the classifier's performance for each land use type. The accuracy in Table 3(a)-(b) reveals that the training dataset outperformed the validation dataset by 5.79% (barren land), 7.01% (built-up area), 15.3% (coal area), 5.66% (vegetation), and 5.73% (waterbody). Similarly, the precision indices indicate that the training dataset surpassed the validation dataset by 0.16 (barren land), 0.22 (built-up area), 0.18 (coal area), 0.25 (vegetation), and 0.14 (waterbody). In terms of recall, the training dataset outperformed the validation dataset by 0.22 (barren land), 0.29 (coal area), and 0.21 (waterbody). Finally, the F1-score, which provides a balanced measure of performance, showed that the training dataset outperformed the validation dataset by 0.19 (barren land), 0.14 (built-up area), 0.27 (coal area), 0.25 (vegetation), and 0.19 (waterbody).

**Table 3. Confusion matrix demonstrates the classifier's ability to assess the land use types: (a) training dataset and (b) validation dataset.**

| a) For training dataset | | | | | |
|---|---|---|---|---|---|
| **Class** | **Barren land** | **Built-up area** | **Coal area** | **Vegetation** | **Waterbody** |
| **n (truth)** | 37 | 34 | 30 | 39 | 25 |
| **n (classified)** | 43 | 38 | 23 | 39 | 22 |
| **Accuracy** | 96.36% | 97.58% | 94.55% | 100% | 98.18% |
| **Precision** | 0.86 | 0.89 | 0.96 | 1 | 1 |
| **Recall** | 1 | 1 | 0.73 | 1 | 0.88 |
| **F1 Score** | 0.93 | 0.94 | 0.83 | 1 | 0.94 |
| **b) For validation dataset** | | | | | |
| **Class** | **Barren land** | **Built-up area** | **Coal area** | **Vegetation** | **Waterbody** |
| **n (truth)** | 9 | 10 | 16 | 9 | 9 |
| **n (classified)** | 10 | 15 | 9 | 12 | 7 |
| **Accuracy** | 90.57% | 90.57% | 79.25% | 94.34% | 92.45% |
| **Precision** | 0.70 | 0.67 | 0.78 | 0.75 | 0.86 |
| **Recall** | 0.78 | 1 | 0.44 | 1 | 0.67 |
| **F1 Score** | 0.74 | 0.80 | 0.56 | 0.75 | 0.75 |

In this study, there have utilized ANNs model to estimate the area of LU classes in the mining activity regions of a sub-part of Angul District in Odisha, India. The spatial features of interest are the AOI derived from 10-meter resolution Sentinel-2A satellite data. The LU classes of interest are those which are typically associated with mining activities such as barren land, water bodies, vegetation, and built-up areas. Also the use of ANNs in this study allows for the estimation of the area of the various LU classes with a high degree of accuracy. This is particularly important in mining activity regions where accurate estimation of the extent of barren land or other land use types

can inform land management and conservation strategies.

It's employed a quantitative analysis approach as described in [50]. This involved determining the proportions of pixels within the AOI that contained each LU class, which provides valuable information on the extent of each class within the study area. The resulting classified classes are presented in Figure 7 (a), which shows the spatial distribution of the various LU classes in the study area. The use of RGB bands in the Sentinel-2A data allowed for the clear visualization and classification of the different LU classes, which include barren land, water bodies, vegetation, and built-up areas.

It utilized a patch-based approach. Each patch contained a group of 10 by 10 pixels, and the AOI was divided into 640 by 1080 patches in total. By converting pixels to area using the sensing resolution of the Sentinel 2-A data, there were able to estimate the total area of the AOI. Specifically, the area of each patch was determined by multiplying the area represented by a single pixel by the number of pixels in the patch. This resulted in an AOI area of {(640*1080) *(10*10) *10} $m^2$, or approximately 691.2 $km^2$. The use of a patch-based approach allowed for the accurate estimation of the area of each LU class within the AOI, which is particularly important in areas undergoing rapid land-use changes, such as mining activity regions. The resulting area estimates provide valuable information for land management and conservation strategies, as well as informing policy decisions related to land use and development.

The histogram map of LU in year 2019 coverage in percentage wise each class is illustrated in Figure 7 (b) shows that the LU classification among five class viz. Coal mining area ~5%, vegetation area ~24%, Water body area ~ 6%, Built-up area ~ 25%, Barren land area ~ 26%, and unclassified area remaining ~ 14%.

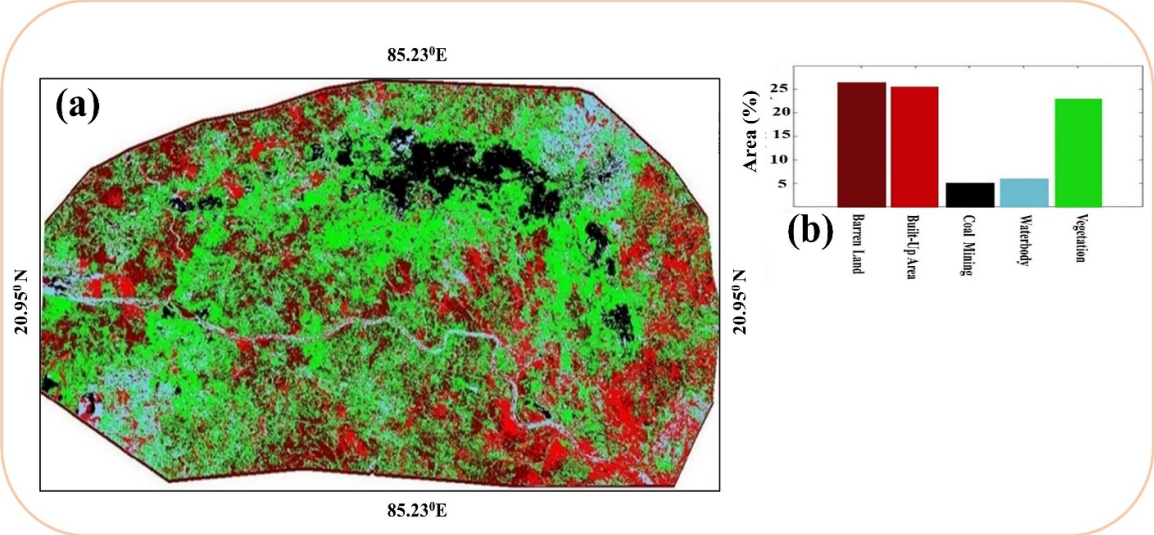


**Figure 7. Estimation of the classifier: (a) Land use map of Talcher coalfield located in Angul district of Odisha state, and (b) Land use percentage coverage of different class.**

## 4. Conclusions

In this study, it applied the practices of ANNs based remote sensing image analysis for the pattern classification of mining activities regions into five distinct classes, namely Coal mining area, Vegetation area, Water body area, Built-up area, and Barren land area. The use of ANNs in this context allowed for efficient and accurate classification of the satellite data, which is particularly important for mapping land use patterns in mining activity regions where rapid land-use changes are occurring. Our findings indicate that the ANNs model performed exceptionally well, achieving promising results with fast execution times. Furthermore, the accuracy assessment of the LU map demonstrated a determination ability of up to 79.4%, which highlights the model's potential for accurately classifying land use types in the study area. The future scope for the utilization of the model has significant potential moving forward. It strongly advises you to continue optimising your system so that it processes faster and more accurately. For evidence of the model's flexibility, it may be necessary to undertake further testing on larger

datasets and compare the results from many models. Insightful knowledge on using ANNs for remote sensing image processing in mining activity areas may be gained from this research. More importantly, it highlights the possibility of these methods contributing to efficient land-use management and conservation policies in locations that land-use is changing rapidly.

## References

[1]. Banerjee, N. N., Ed. Trace metals on Indian coals. Allied Publishers, 2000.

[2]. Zhang, C., Sargent, I., Pan, X., Li, H., Gardiner, A., Hare, J., and Atkinson, P.M., An object-based convolutional neural network (OCNN) for urban land use classification. *Remote sensing of environment, 2018, 216,* pp.57-70.

[3]. Pesaresi, M., Huadong, G., Blaes, X., Ehrlich, D., Ferri, S., Gueguen, L., Halkia, M., Kauffmann, M., Kemper, T., Lu, L., and Marin-Herrera, M.A., A global human settlement layer from optical HR/VHR RS data: Concept and first results. *IEEE Journal of Selected Topics in Applied Earth Observations and Remote Sensing, 2013, 6(5),* pp. 2102-2131.

[4]. Wang, L., Sousa, W.P., and Gong, P., Integration of object-based and pixel-based classification for mapping mangroves with IKONOS imagery. *International journal of remote sensing, 25(24),* 2004, pp. 5655-5668.

[5]. Weih, R.C. and Riggan, N.D., Object-based classification *vs.* pixel-based classification: Comparative importance of multi-resolution imagery. *The International Archives of the Photogrammetry, Remote Sensing and Spatial Information Sciences, 2010, 38(4),* p.C7.

[6]. Schalkoff, Robert J. Digital Image Processing and Computer Vision: An Introduction to Theory and Implementations. *John Wiley & Sons, Inc., 1989.*

[7]. Kamavisdar, P., Saluja, S., and Agrawal, S., A survey on image classification approaches and techniques. *International Journal of Advanced Research in Computer and Communication Engineering, 2013, 2(1),* pp. 1005-1009.

[8]. Carvajal, F., E. Crisanto, F. J. Aguilar, F. Agüera, and M. A. Aguilar. "Greenhouses detection using an artificial neural network with a very high resolution satellite image." *In ISPRS Technical Commission II Symposium, Vienna, 2006*, pp. 37-42.

[9]. Hepner, G., Logan, T., Ritter, N., and Bryant, N., Artificial neural network classification using a minimal training set-Comparison to conventional supervised classification. *Photogrammetric Engineering and Remote Sensing, 1990, 56(4),* pp. 469-473.

[10]. Zhang, L., Zhang, L., Du, B., You, J., and Tao, D., 2019. Hyperspectral image unsupervised classification by robust manifold matrix factorization. *Information Sciences, 485, pp*. 154-169.

[11]. Bruzzone, L., Chi, M., and Marconcini, M., A novel transductive SVM for semisupervised classification of remote-sensing images. *IEEE Transactions on Geoscience and Remote Sensing, 2006, 44(11), pp*. 3363-3373.

[12]. François-Lavet, Vincent, Yoshua Bengio, Doina Precup, and Joelle Pineau. "Combined reinforcement learning via abstract representations." *In Proceedings of the AAAI Conference on Artificial Intelligence, 2019, Vol*. 33, No. 01, pp. 3582-3589.

[13]. Khatami, R., Mountrakis, G. and Stehman, S.V., A meta-analysis of remote sensing research on supervised pixel-based land-cover image classification processes: *General guidelines for practitioners and future research. Remote Sensing of Environment, 2016, 177,* pp. 89-100.

[14]. McCulloch, W.S. and Pitts, W., A logical calculus of the ideas immanent in nervous activity. *The bulletin of mathematical biophysics, 1943, 5(4),* pp. 115-133.

[15]. Rosenblatt, F., The perceptron: a probabilistic model for information storage and organization in the brain. Psychological review, 1958, 65(6), p. 386.

[16]. Werbos PJ, Back-propagation through Time : What It Does and How to Does It. 1990, Vol. 78, pp. 1550–1560.

[17]. Ackley DH, Hinton GE, and Sejnowski TJ , A learning algorithm for Boltzmann machines. *Cogn Sci, 1985, Vol. 9, pp.* 147–169.

[18]. Tan K, Wu F, and Du Q, A parallel gaussian--bernoulli restricted boltzmann machine for mining area classification with hyperspectral imagery. *IEEE J Sel Top Appl Earth Obs Remote Sens , 2019, Vol.12, pp.* 627–636.

[19]. Lin Y, Lv F, and Zhu S, Large-scale image classification: Fast feature extraction and SVM training. *In: CVPR, 2011, pp 1689–1696.*

[20]. Bahroun Y and Soltoggio A , Online representation learning with single and multi-layer Hebbian networks for image classification. *In: International Conference on Artificial Neural Networks, 2017,* pp 354–363.

[21]. Fred ALN and Jain AK, Combining multiple clusterings using evidence accumulation. *IEEE Trans Pattern Anal Mach Intell, 2005, Vol. 27, pp*. 835–850.

[22]. Andrews H and Patterson C, Singular value decomposition (SVD) image coding. *IEEE Trans Commun, 1976, Vol. 24, pp*. 425–432.

[23]. Zhu L, Chen Y, Ghamisi P, and Benediktsson JA, Generative adversarial networks for hyperspectral image classification. *IEEE Trans Geosci Remote Sens, 2018, Vol. 56, pp*. 5046–5063.

[24]. Fraley C, Algorithms for model-based Gaussian

hierarchical clustering. *SIAM J Sci Comput , 1998, Vol. 20, pp.* 270–281.

[25]. Rodarmel C and Shan J, Principal component analysis for hyperspectral image classification. *Surv L Inf Sci, 2002, Vol. 62, pp.* 115–122.

[26]. Li X and Guo Y, Adaptive active learning for image classification. *In: Proceedings of the IEEE Conference on Computer Vision and Pattern Recognition, 2013, pp* 859–866.

[27]. Som S and Sen S, A non-adaptive partial encryption of grayscale images based on chaos. *Procedia Technol, 2013, Vol. 10, pp.* 663–671.

[28]. Akyuz E, Ilbahar E, Cebi S, and Celik M, Maritime environmental disaster management using intelligent techniques. In: Intelligence Systems in Environmental Management: *Theory and Applications. Springer, 2017, pp 135–155.*

[29]. Gayen A, Pourghasemi HR, and Saha S, Gully erosion susceptibility assessment and management of hazard-prone areas in India using different machine learning algorithms. *Sci Total Environ, 2019, Vol. 668, pp.* 124–138.

[30]. Basheer IA and Hajmeer M, Artificial neural networks: fundamentals, computing, design, and application. *J Microbiol Methods, 2000, Vol. 43, pp.* 3–31.

[31]. Guo H, Nguyen H, Vu D-A, and Bui X-N, Forecasting mining capital cost for open-pit mining projects based on artificial neural network approach. *Resour Policy, 2019, 101474*.

[32]. Zhao W and Du S , Spectral--spatial feature extraction for hyperspectral image classification: A dimension reduction and deep learning approach. *IEEE Trans Geosci Remote Sens, 2016, Vol. 54, pp 4544–4554.*

[33]. Huang WY and Lippmann RP, Neural net and traditional classifiers. *In: Neural information processing systems, 1988, pp 387–396.*

[34]. El Mouatasim, A., Fast gradient descent algorithm for image classification with neural networks. *Signal, Image and Video Processing, 2020, Vol. 14, Issue 8, pp. 1565-1572.*

[35]. Kanellopoulos I, Wilkinson GG, and Megier J, Integration of neural network and statistical image classification for land cover mapping. *In: Proceedings of IGARSS'93-IEEE International Geoscience and Remote Sensing Symposium, 1993, pp 511–513*.

[36]. Mishra N, Research Study on Coal Mining, Displacement and Rural Livelihoods: A Study in Mahanadi Coalfield Odisha, 2019.

[37]. Li J, Liu Z, and Liu S, Suppressing the image smear of the vibration modulation transfer function for remote-sensing optical cameras. *Appl Opt , 2017, Vol. 56, pp.* 1616–1624.

[38]. Thornton MW, Atkinson PM, and Holland DA, Sub-pixel mapping of rural land cover objects from fine spatial resolution satellite sensor imagery using super-resolution pixel-swapping. *Int J Remote Sens, 2006, Vol. 27, pp. 473–491.*

[39]. Arif M, Suresh M, Jain K, and Dundhigal S, Sub-pixel classification of high resolution satellite imagery. *Int J Comput Appl, 2015, Vol. 129.*

[40]. Hester DB, Cakir HI, Nelson SAC, and Khorram S , Per-pixel classification of high spatial resolution satellite imagery for urban land-cover mapping. *Photogramm Eng Remote Sens, 2008, Vol. 74, pp. 463–471.*

[41]. Bollman JE, Rao RL, Venable DL, and Eschbach R, Automatic image cropping, 1999.

[42]. Kortchagine DN and Krylov AS, Projection filtering in image processing. *In: Proc. of the Int. Conf. Graphicon, 2000, pp 42–45.*

[43]. Petrov AA, Dosher BA, and Lu Z-L,The dynamics of perceptual learning: an incremental reweighting model. *Psychol Rev, 2005, Vol. 112, p 715.*

[44]. Marmarelis VZ and Zhao X, Volterra models and three-layer perceptrons. *IEEE Trans Neural Networks, 1997, Vol. 8, pp. 1421–1433.*

[45]. Vasilyev AN and Tarkhov DA, Mathematical models of complex systems on the basis of artificial neural networks, 2014.

[46]. Gomes GS da S and Ludermir TB, Optimization of the weights and asymmetric activation function family of neural network for time series forecasting. *Expert Syst Appl, 2013, Vol. 40, pp. 6438–6446.*

[47]. Li J, Cheng J, Shi J, and Huang F, Brief introduction of back propagation (BP) neural network algorithm and its improvement. In: Advances in computer science and information engineering. *Springer, 2012, pp 553–558.*

[48]. Bottou L, Stochastic gradient learning in neural networks. Proc Neuro-N{\i}mes, 1991, Vol. 91, Issue12.

[49]. Hughes M, Bygrave J, Bastin L, and Fisher P, High order uncertainty in spatial information: estimating the proportion of cover types within a pixel. *Spat Accuracy Assess L Inf Uncertain Nat Resour, 1999, pp. 319–323.*

[50]. Kumar A, Gupta A, Singh YP, and Bhagat M. A Deep Neural Network for Classification of Land Use Satellite Datasets in Mining Environments. *Journal of Mining and Environment. 2022 Jul 1;13(3):797-808.*

[51]. Alshari EA, Abdulkareem MB, and Gawali BW. Classification of land use/land cover using artificial intelligence (ANN-RF). *Frontiers in Artificial Intelligence. 2023;5:964279.*

[52]. Debnath M, Islam N, Gayen SK, Roy PB, Sarkar B, and Ray S. Prediction of spatio-temporal (2030 and

2050) land-use and land-cover changes in Koch Bihar urban agglomeration (West Bengal), India, using artificial neural network-based Markov chain model. *Modeling Earth Systems and Environment. 2023 2:1-22.*

[53]. Lukas P, Melesse AM, and Kenea TT. Prediction of future land use/land cover changes using a coupled CA-ANN model in the upper omo–gibe river basin, Ethiopia. *Remote Sensing. 2023;15(4):1148.*

[54]. Girma R, Fürst C, and Moges A. Land use land cover change modeling by integrating artificial neural network with cellular Automata-Markov chain model in Gidabo river basin, main Ethiopian rift. *Environmental challenges. 2022 Jan 1;6:100419.*

[55]. Kumar S, Shwetank S, and Jain K. Development of spectral signature of land cover and feature extraction using artificial neural network model. *In 2021 International Conference on Computing, Communication, and Intelligent Systems (ICCCIS) 2021 (pp. 113-118). IEEE.*

[56]. Olson, D.L. and Delen, D., Performance evaluation for predictive modeling. In: Advanced Data Mining Techniques. 2008.

# یک سیستم خودکار امیدوارکننده برای مطالعه سطوح معادن زغالسنگ با استفاده از داده‌های Sentinel-2 برای ارزیابی طبقه‌بندی بر اساس الگوی مبتنی بر پیکسل

**آجی کومار**

**گروه علوم و مهندسی کامپیوتر، دانشکده علوم و مهندسی کامپیوتر، دانشگاه مانیپال جیپور، راجستان، هند**

ارسال ۲۰۲۳/۰۵/۰۹، پذیرش ۲۰۲۳/۰۹/۱۹

* نویسنده مسئول مکاتبات: ajay3789@gmail.com

**چکیده:**

طبقه بندی کاربری زمین (LU) بر اساس تصاویر سنجش از دور یک کار چالش برانگیز است که می‌تواند به طور مؤثر با استفاده از یک چارچوب یادگیری مورد توجه قرار گیرد. با این حال، طبقه‌بندی دقیق پیکسل‌ها بر اساس کاربری زمین، مشکل قابل توجهی دارد. با وجود پیشرفت در تکنیک‌های استخراج ویژگی، اثربخشی الگوریتم‌های یادگیری می‌تواند به طور قابل توجهی متفاوت باشد. در این مطالعه که در تالچر، اُدیشا، هند انجام شد، محققان استفاده از شبکه‌های عصبی مصنوعی (ANN) را برای طبقه‌بندی کاربری زمین بر اساس مجموعه داده‌های جمع‌آوری‌شده توسط ماهواره Sentinel-2 پیشنهاد کردند. این مطالعه بر روی منطقه تالچر متمرکز بود که به پنج کلاس کاربری متمایز از زمین تقسیم شد: منطقه زغالسنگ، منطقه ساخته شده، منطقه بایر، منطقه پوشش گیاهی و منطقه آب. هدف محققان با استفاده از شبکه‌های عصبی مصنوعی در منطقه معدنی تالچر، بهبود دقت طبقه‌بندی کاربری زمین بود. نتایج به‌دست‌آمده از مطالعه، دقت کلی ۷۹.۴ درصد را نشان داد. این کار تحقیقاتی اهمیت استفاده از تصاویر سنجش از دور و یک چارچوب یادگیری را برای رسیدگی به چالش‌های مرتبط با طبقه‌بندی کاربری زمین مبتنی بر پیکسل نشان می‌دهد. این مطالعه با استفاده از شبکه‌های عصبی مصنوعی و استفاده از داده‌های ماهواره Sentinel-2، بینش‌های ارزشمندی را برای طبقه‌بندی مؤثر دسته‌های کاربری مختلف در منطقه تالچر هند ارائه می‌کند. یافته‌ها به پیشرفت تکنیک‌ها برای تجزیه و تحلیل دقیق کاربری زمین، با کاربردهای بالقوه در زمینه‌های مختلف مانند برنامه‌ریزی شهری، نظارت بر محیط‌زیست و مدیریت منابع کمک می‌کنند.

**کلمات کلیدی:** حفاظت از زمین، علوم زمین، پدیده جدید، حفاظت، میراث زمین شناسی، ژئوسایت.